Journal of Photochemistry & Photobiology, B: Biology 218 (2021) 112181

Contents lists available at ScienceDirect

Journal of Photochemistry & Photobiology, B: Biology

journal homepage: www.elsevier.com/locate/jphotobiol

Combined photodynamic therapy with chloroaluminum phthalocyanine and doxorubicin nanoemulsions in breast cancer model

Ágata Silva Cabral [a], Ellen Cristina Rivas Leonel [b], Natália Maria Candido [a], Henrique Luis Piva [c], Maryanne Trafani de Melo [c], Sebastião Roberto Taboga [b], Paula Rahal [a], Antonio Claudio Tedesco [c], Marilia Freitas Calmon [a,*]

[a] Laboratory of Genomic Studies, São Paulo State University, São José do Rio Preto, São Paulo 15054-000, Brazil
[b] Laboratory of Microscopy and Microanalysis, São Paulo State University, São José do Rio Preto, São Paulo 15054-000, Brazil
[c] Chemistry Department, Center of Nanotechnology and Tissue Engineering - Photobiology and Photomedicine Research Group, University of São Paulo; Ribeirão Preto, São Paulo 14040-901, Brazil

ARTICLE INFO

Keywords:
Alternative therapy
Anticancer treatment
Breast cancer
Nanotechnology
PDT
Photosensitizer

ABSTRACT

Breast cancer is the most common neoplasm among women but thanks to innovative therapies, patients' prognosis has considerably improved. In this aspect, nanotechnology has been applied for cancer therapy aiming to reduce its usual side effects. In this study we aimed to evaluate the effects of nanoemulsions containing photosensitizer and chemotherapeutic agents associated with photodynamic therapy in a breast cancer *in vivo* model. Our results showed that synergistic treatments in which chloroaluminum phthalocyanine (NE-Pc) administered together with Doxorubicin (Dox) in the presence of laser irradiation (NE-PcDoxo + PDT) led to a reduction of 4 T1 induced breast cancer in mice, decline of tumor VEGF expression, increase in Caspase-3 expression, tissue necrosis and massive decrease in proliferative cells, as shown by Ki67 immunostaining. Furthermore, this associated treatment induced overexpression of apoptotic genes *ABL1*, *CD70*, *CRADD*, *FASL*, and *NME5* and a reduction in expression of anticancer drug target genes *CDK2, ERBB2, FIGF, IGF2, PARP4* and *PGR*. These results validate this treatment as a promising alternative to improve the currently applied anticancer strategies.

1. Introduction

Female breast cancer (BC) has been diagnosed in 2.1 million women in 2018 causing more than 626,679 deaths in that year and representing 18.4% of total cancer deaths worldwide [1]. Depending on the subtype, stage, histopathology or gene expression, current treatment options consist of locoregional surgery or complete mastectomy, radiation therapy, systemic chemotherapy, hormonal therapy, or immunotherapy. Although chemotherapy successfully prolongs life span of patients, anticancer drugs have several limitations and side effects. In addition, unspecific drug pharmacokinetics may take place and patients may develop chemoresistance to treatment [2].

Nanotechnology is suggested to reduce the treatment dosage and frequency due to the nanocarrier's ability to deliver the drug within confined tissues and versatile materials have been applied to encapsulate chemotherapeutic agents [3]. In this context, nanoemulsions are used due to their fluid nature and well-established interaction with tissue cells, in which the oil phase plays a vital role solubilizing lipophilic drugs molecules ensuring sustained and controlled drug release for long periods [4].

Photodynamic Therapy (PDT) has proved to be a powerful strategy in tumor destruction and this treatment modality applies visible light to induce a cascade of events leading the PS to the excited triplet state, generating reactive oxygen species (ROS) which cause tumor cell death [5]. The most important benefit of PDT are the selective ability that limits the area to be exposed to the light and accumulation of the PS in the tumor region, attributed to low pH, increased vascular permeability, poor lymphatic drainage, and distorted stromal architecture of the tumor [6].

Chloroaluminum phthalocyanine (AlClPc) and derivatives have

* Corresponding author at: Department of Biology, Instituto de Biociências, Letras e Ciências Exatas – IBILCE/UNESP, Cristóvão Colombo, 2265, 15054-000 São José do Rio Preto, SP, Brazil.
E-mail address: marilia.calmon@unesp.br (M.F. Calmon).

https://doi.org/10.1016/j.jphotobiol.2021.112181
Received 21 August 2020; Received in revised form 12 March 2021; Accepted 22 March 2021
Available online 24 March 2021

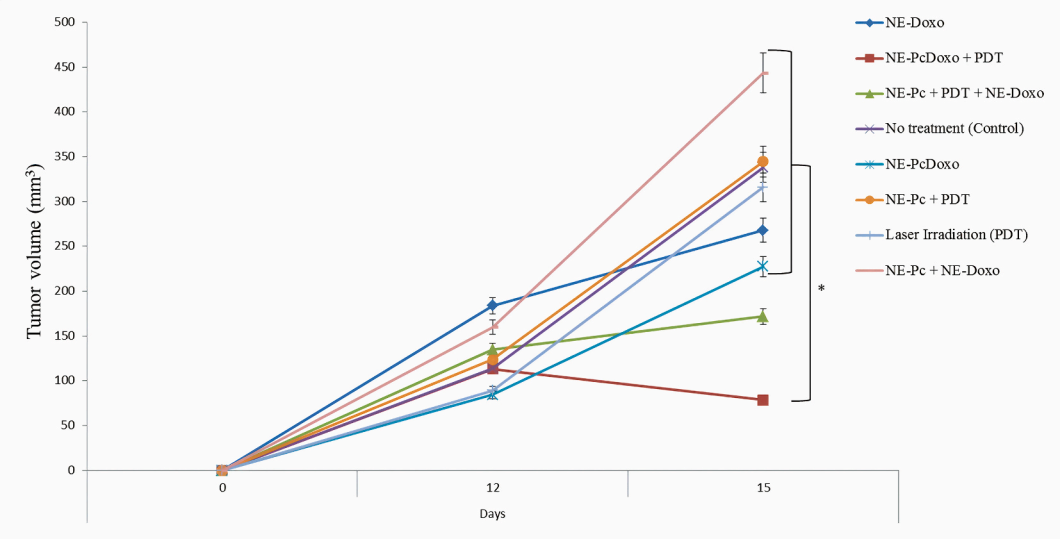

Fig. 1. Tumor growth curves in the evaluated groups from the day experiment started (day 0) and the day of euthanasia (day 15). * $p < 0.01$.

attracted attention due their optimal characteristics for anticancer PDT, such as light absorption inside the "therapeutic window" (600–770 nm) that allows maximum penetration and less damaging to the tissue. However, phthalocyanines have high hydrophobicity and self-aggregation under physiological conditions, so, different strategies are used to modify their chemical structure or encapsulate them in nano-carriers [7].

Doxorubicin (DOX) is frequently applied for BC but presents chemical instability being a challenge for storage, handling, and treatment efficacy. On the other hand, the application of free drug is related to multiple resistance associated with adaptive cellular mechanisms and mutations, changes in signaling pathways, increased efflux in tumor cells, dose-dependent cardiotoxicity in addition to have slow and limited tissue absorption [8]. Clinical cases and animal studies suggests that chemotherapy is more effective when multiple drugs are administered in combination to obtain synergy, enhancing the therapeutic benefits against cancer [9,10]. The use of nanoemulsions as carriers of photosensitizers associated with chemotherapy is an attractive alternative, especially when combined with PDT. So, this work aimed to evaluate nanoemulsion effects containing AlClPc and Doxorubicin associated with PDT in the breast cancer *in vivo* model.

2. Material and Methods

2.1. Synthesis of Nanostructured Systems and PDT Apparatus

Nanostructured systems obtained by spontaneous emulsification based on the modified method described by Tabosa do Egito [11] were used: nanoemulsions containing chloroaluminum phthalocyanine (NE-Pc), doxorubicin (NE-Doxo) and both drugs (NE-PcDoxo). For NE-Pc, the organic phase (acetone) was prepared using medium-chain triglycerides, natural soy phospholipids (Liposoid S100, Lipid Co, Brazil), and ClAlPc (Sigma-Aldrich, USA) at 55 °C. Subsequently, this organic solution was added to the aqueous phase containing an anionic surfactant and poloxamer 188 (Sigma-Aldrich, USA) under magnetic stirring. Organic solvent was removed entirely by route-evaporation under reduced pressure at 60 °C. For NE-Doxo, a similar preparation took place except for the addition of the photosensitizer, and doxorubicin was added to the aqueous phase. Additionally, for NE-PcDoxo, both drugs were added to the final formulation, according to the protocol adopted [12]. All samples were prepared under aseptic conditions in the absence of contaminants and chemical interference. Three sessions of visible light irradiation at 630 nm of 50 J.cm^{-2} were applied in separate experimental groups using continuous laser Eagle 2 W at 60 mW (Quantum Tech, São Carlos, Brazil) with an interval of 24 h between each session.

2.2. In Vivo Experimental Model

The murine BC cell line (4 T1) acquired from ATCC was cultured in Roswell Park Memorial Institute medium (RPMI1640) (GIBCO-BRL, Life Technologies, USA) supplemented with 10% fetal bovine serum (FBS) (Cultilab, Brazil), 100 U/mL penicillin (GIBCO-BRL, Life Technologies, USA), and 100 g/mL streptomycin (GIBCO-BRL, Life Technologies, USA). The cells were maintained in a humidified 5% CO_2 incubator and a constant temperature of 37 °C.

Forty female BALB/c mice (6 to 8 weeks) were kept under-ventilated cages and maintained in the Animal Breeding Center of the Institute of Biosciences, Humanities, and Exact Sciences (IBILCE) of São Paulo State University (UNESP). Environment temperature (24 ± 2 °C) and luminosity (12 h light/dark cycle) were controlled, and animals received specific balanced feed (Presence, Paulínia, Brazil) and fresh filtered water *ad libitum*. The experimental design was conducted according to the Ethics Committee on the Use of Animals (CEUA) from IBILCE/UNESP under the protocol n° 081/2013. The animals were divided into 8 groups ($n = 5$), with animals being kept as a control group, tumor cells were inoculated, and no treatment was applied. In the rest of the animals, 2×10^5 4 T1 cells diluted in 100 μL of phosphate-saline buffer (PBS) were inoculated in the fourth right mammary gland, aiming the development of a tumor at the injection site and were daily monitored until the end of the experiment. On the 12th day after tumor cells grafting, and with the tumor being clinically apparent (palpable), the treatments were performed as follows: Intratumoral injection of 100 μL nanoemulsions (1 μM of chloroaluminum phthalocyanine associated/or 0.5 μM of doxorubicin diluted in 0.9% NaCl) was administered once associated or not with PDT sessions every 24 h during three days in the animals under anesthesia (Rompun, Bayer, Brazil; Dopalen, Ceva, Brazil). Briefly, the animals with 4 T1 breast tumor were divided into groups: **1** - NE-Doxo administration in the first day of the treatment without PDT sessions (NE-Doxo); **2** - NE-PcDoxo administration in the first day of the treatment associated with photodynamic therapy sessions (NE-PcDoxo + PDT); **3** - NE-Pc administration in the first day of the treatment associated with photodynamic therapy sessions and NE-Doxo administration 24 h after the first PDT session (adjuvant treatment) (NE-Pc + PDT + NE-Doxo); **4** – animals without any treatment (Control); **5** - NE-PcDoxo administration without PDT sessions (NE-PcDoxo); **6** - NE-Pc

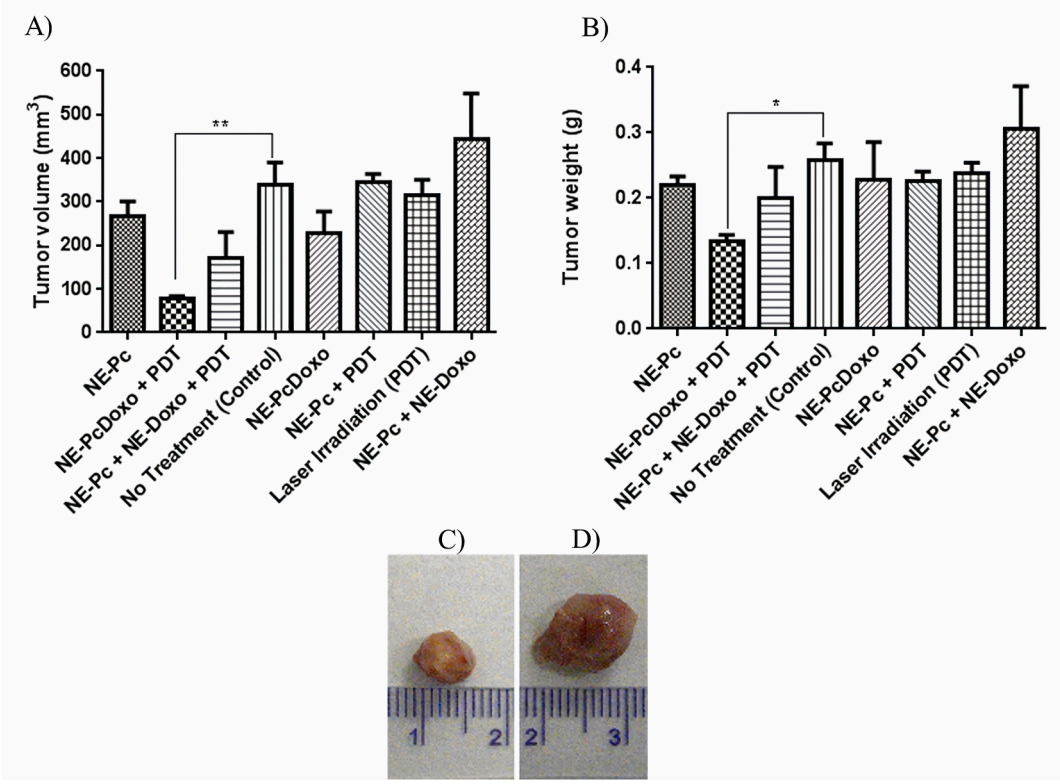

Fig. 2. **(A)** Breast tumor volume of murine after euthanasia among different treatments applied. **(B)** Tumor weight after euthanasia. **(C)** Macroscopic aspect of a tumor treated with NE-PcDoxo + PDT showing a significant decrease in relation to the **(D)** 4 T1 control mammary tumor (without treatment). Significant *p*-value in the ANOVA test followed by Kruskal-Wallis (± S.E.M. * = $p < 0.01$ and ** = $p < 0.001$ in comparison to control group).

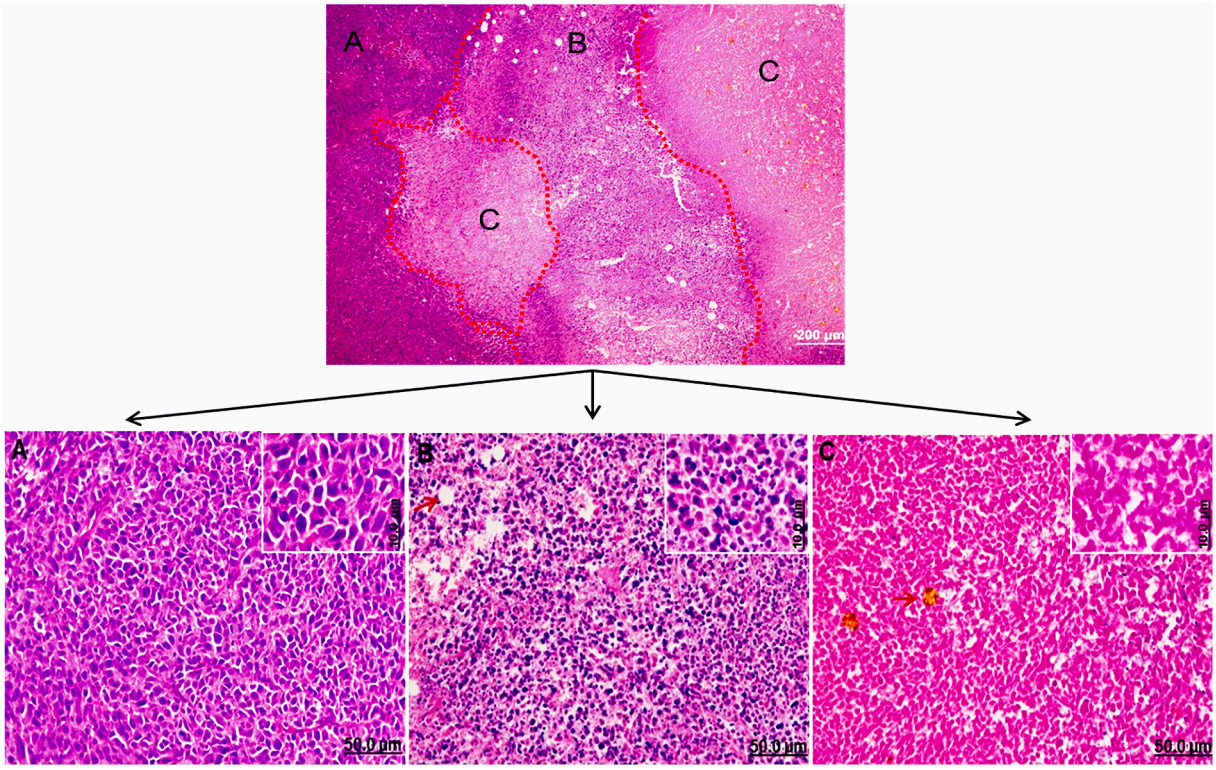

Fig. 3. Histological section of tumor tissue from animal treated with NE-PcDoxo + PDT. **(A)** Peripheral tumor region with prevalence of proliferative cells. **(B)** Initial necrosis with evidence of pyknotic nuclei and formation of cribriform patterns (arrow). **(C)** Advanced stage of tissue necrosis showing karyolysis and hemosiderin deposits (arrow). Main figure: 4× magnification, scale bar 200 µm. A, B and C: 20× (main figures, scale bars of 50 µm) and 100× magnification (panels, scale bars of 10 µm).

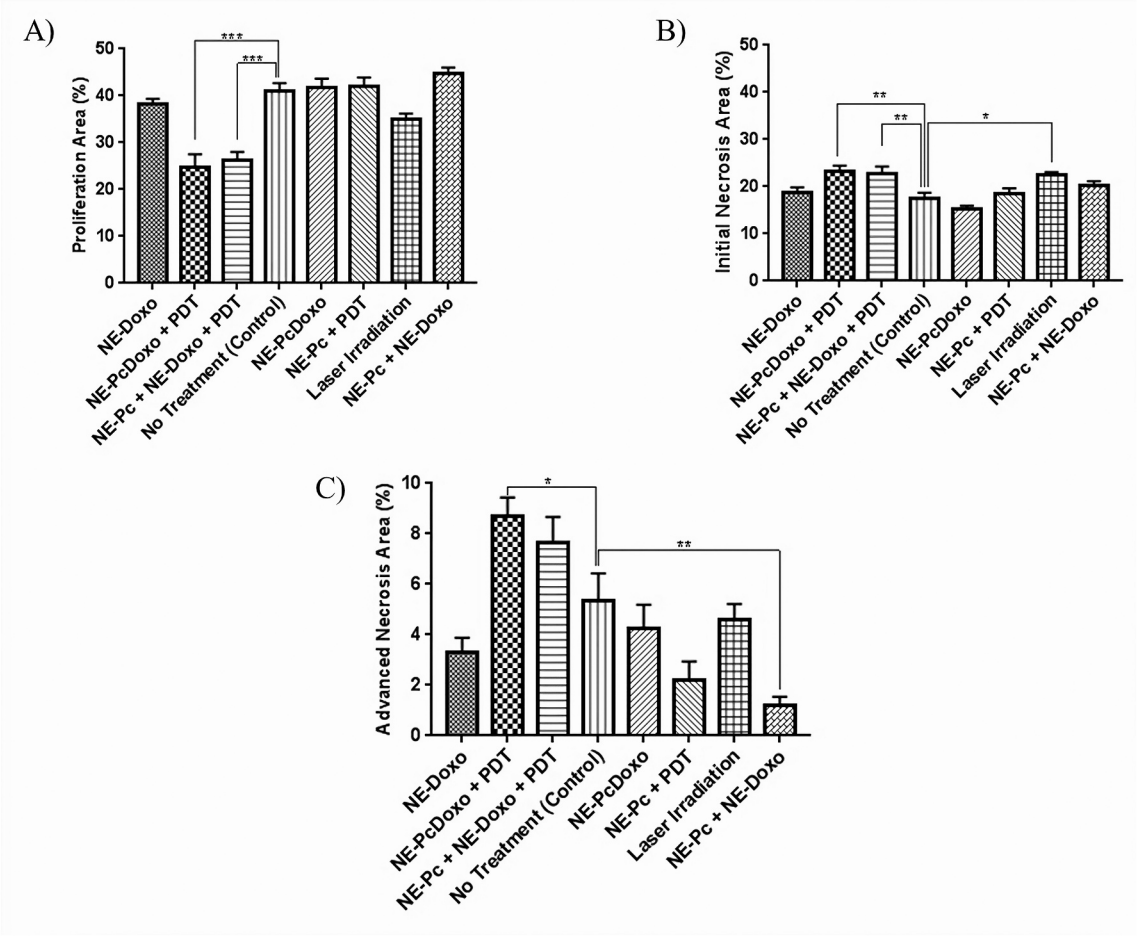

Fig. 4. Stereological data of 4 T1 strain mammary tumors subjected to different treatments. **A)** Proliferative areas; **B)** Initial necrotic areas; **C)** Advanced necrotic areas. Significant *p*-value in the ANOVA test followed by Bonferroni (±S.E.M * = $p < 0.01$; ** = $p < 0.001$; *** = $p < 0.0001$ compared to control group).

administration in the first day of the treatment associated with photodynamic therapy sessions (NE-Pc + PDT); **7** - treated with laser irradiation; **8** - NE-Pc administration in the first day of the treatment and NE-Doxo administration after 24 h (adjuvant treatment) without PDT sessions (NE-Pc + NE-Doxo). Measurements of the tumor diameters were made on the day 12 (beginning of treatments) and 15 with the aid of a caliper. The animals were euthanized on the 15th day (stunning performed by CO_2 followed by decapitation) 24 h after the last PDT session, and tumors were collected.

After euthanizing the animals, tumor samples were taken from all animals and histologically processed. For paraffin processing (Histosec, Merck), fixation in paraformaldehyde 4% was carried out at 4 °C. Samples were then dehydrated in an increasing series of ethanol, diaphanized in xylol, and included in paraffin. The blocks were subjected to 5 μm slices on a rotating microtome (Leica RM2155, Germany), proceeding to HE staining for appropriate histopathological evaluation of the tissues.

2.3. PDT Efficiency Combined with Nanoemulsions

The anti-tumor efficiency was analyzed by comparing tumor growth between groups before and after the treatments. The Kaplan-Meier method was used to estimate the time of tumor expansion for each group. Tumor growth was visually identified from the 7th day of 4 T1 cells inoculation. Different treatments started on the 12th day, and the animals were euthanized on the 15th day. Tumor weight was assessed after euthanasia and volume along the experiment were measured according to the formula:

$$mm^3 = 0.52 \text{ x L (Length) x } W^2\text{(Width)} \quad (1)$$

2.4. Immunohistochemical Assays

Expose Rabbit Specific HRP/DAB Detection Kit (ab80437 Abcam, UK) was used. The slides were deparaffinized in xylol and rehydrated in a decreasing series of ethanol. Soon after, they were washed with distilled water for 5 min and kept for 45 min in a steam pan at 96 °C with citrate buffer (pH 6.0) for antigenic recovery. After stabilization at room temperature, the slides were washed with TBS buffer (3x5min) and incubated with 0.1% H_2O_2 solution ready for use (hydrogen peroxide block) for 10 min. After a new wash with TBS (2x5min), a ready-to-use protein blocking solution was added for 10 min as described by the manufacturer, and later the slides were rewashed in TBS buffer (2x5min). In the end, the slides were incubated with rabbit polyclonal primary antibodies Ki67 (1:500, ab15580, Abcam, UK), activated Caspase-3 (1:100, ab13847, Abcam, UK), VEGF (1:100, ab46154, Abcam, UK) or CD31 (1:50, ab28364, Abcam, UK) diluted in 1% albumin and kept at 4 °C overnight. The slides were then washed in TBS buffer (3x5min) and incubated with the specific secondary conjugate HRP rabbit for 30 min. Revelation was carried out with a chromogenic substrate DAB (3,3′-diaminobenzidine tetrahydrochloride) and counterstained with hematoxylin.

For evaluation of VEGF and Caspase-3 expression, ImageJ software (version 1.52, Bethesda MD, NIH, USA) was applied. The slides were digitized using a BX-60 optical microscope (Olympus, Japan) coupled to a computer with the DP-BSW V3.1 software (Olympus, Japan), and 10

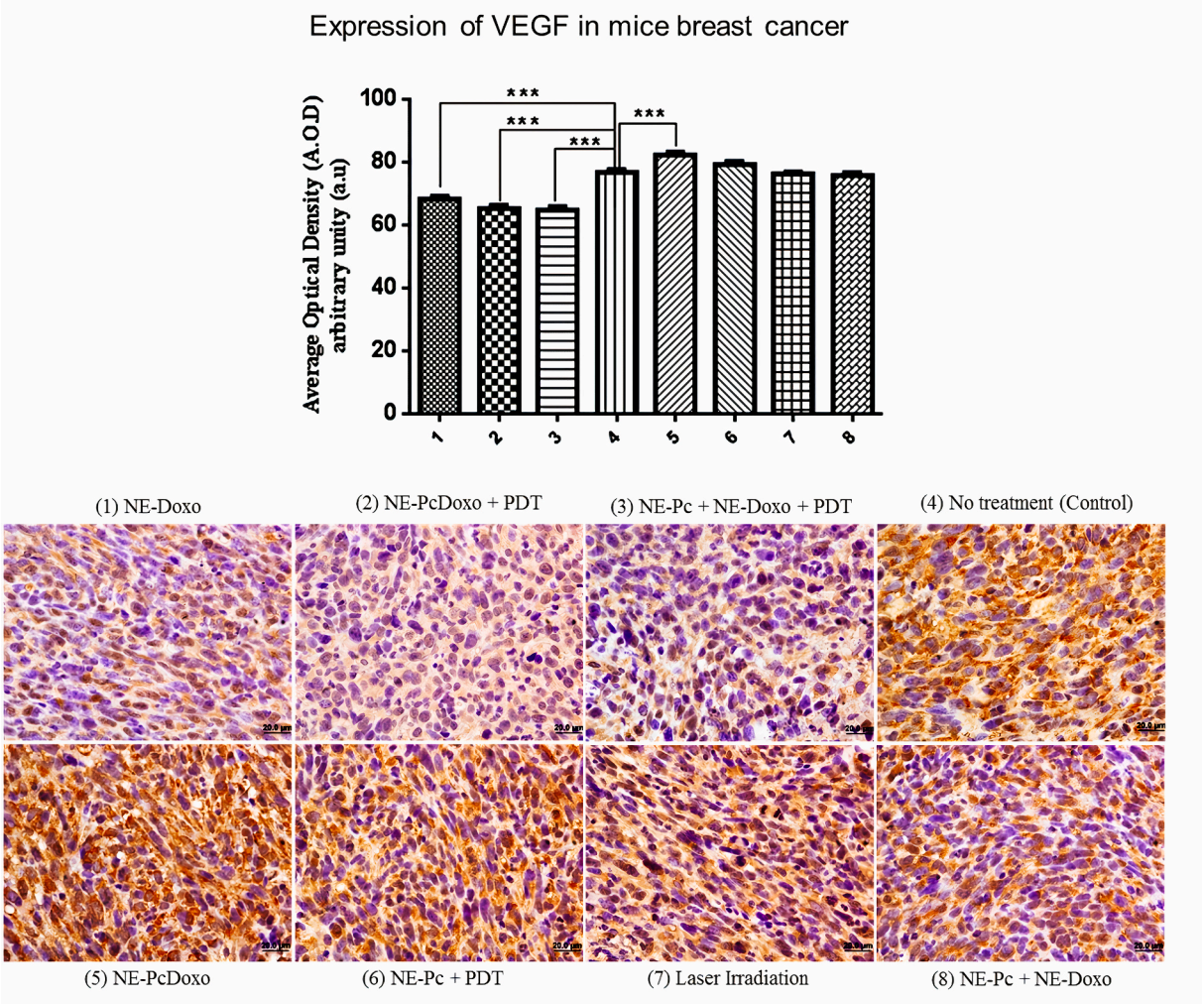

Fig. 5. VEGF expression in tumors from animals of the control group and subjected to different treatments. Micrographs in 40× magnification (Bars in 20 μm scale). Significant *p*-value in the ANOVA test followed by Bonferroni (± S.E.M. *** = $p < 0.0001$ compared to the control group). Legends: (1) NE-Doxo: nanoemulsion with doxorubicin without PDT sessions; (2) NE-PcDoxo + PDT: nanoemulsion containing chloroaluminum phthalocyanine and doxorubicin associated with photodynamic therapy; (3) NE-Pc + PDT + NE-Doxo: nanoemulsion containing chloroaluminium phthalocyanine associated with photodynamic therapy and 24 h later administration of nanoemulsion containing doxorubicin - after the first PDT session; (4) Control 41 breast cancer mice; (5) NE-PcDoxo: nanoemulsion containing chloroaluminum phthalcianine and doxorubicin without PDT sessions; (6) NE-Pc + TFD: nanoemulsion containing chloroaluminum phthalocyanine associated with photodynamic therapy; (7) Laser Irradiation; (8) NE-Pc + NE-Doxo: nanoemulsion containing chloroaluminum phthalocyanine and 24 h later administration of nanoemulsion containing doxorubicin without PDT sessions.

random photomicrographs were captured using a 40× objective. In each acquired field, 20 points were randomly scored, totaling 200 points, referring to the average intensity of immunostaining for each animal, according to Jardim-Perassi et al. [13]. Values were obtained as arbitrary units (a.u) and represented by mean optical densitometry.

CD31 expression analysis was performed using ImageJ software, and 10 immunoreactive visual fields in 40× magnification were captured. Color deconvolution was applied using a macro that defines hematoxylin and DAB vectors in the software to isolate the DAB stain from the image contrast, as described by Bouzin et al. [14]. The same parameters were applied to all slides. The results were expressed as Staining Index (SI) according to the following formula:

$$S.I = (\text{Annotation ratio}) \times (\%\text{Stained area}) \times (\text{Staining intensity}) \quad (2)$$

*Where: the annotation ratio is the percentage of the outlined area of each field obtained from the tumor, % of the stained area is calculated as (stained area/tissue area)*100, and the staining intensity is calculated as (255-average intensity of colored pixels).

Ki67 expression evaluation was performed by the average of marked cells proportion (%). Twenty random visual tumor fields from each animal were acquired with a 100× objective under the bright field microscope as mentioned above and analyzed using Image-Pro Plus 6.1 software (Media Cybernetics Inc., Silver Spring, MD, USA). The parameter used to define Ki67 expression was the presence of nuclear staining, where positive and negative cells for all photographed visual fields were manually quantified.

2.5. Stereological Analysis

Five cross-sections from the central and peripheral regions of the tumors were stained with H&E. The slides were digitized in 10× magnification using a BX61VS camera (Olympus, Japan) coupled to an Olympus VS120 Virtual Microscope Slide Scanning System (VS120-S5) from the same company and analyzed in an imaging system with the Image-Pro Plus 6 software using the proposed M130 multipoint system by Weibel [15]. This method using the software's grid mask tool was applied to chosen slices from the tumors of each animal, so that 25 images per group were analyzed by this method. The percentage index of proliferation, initial necrosis, advanced necrosis, cribriform pattern, adjacent tissues, and space was noted, being of interest for this study, the

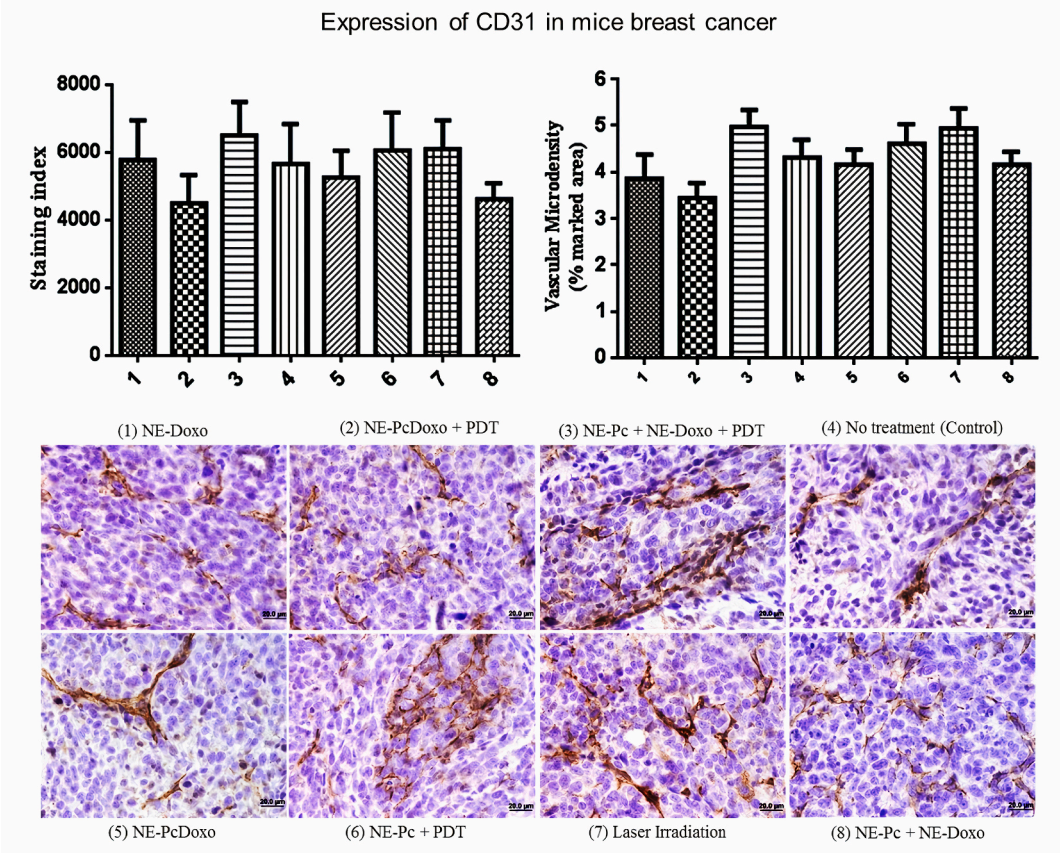

Fig. 6. Vascular microdensity (MDV) by staining index and the % of marked area shown by the expression of CD31 in tumor tissue of the animals from control group and subjected to different treatments. Micrographs in 40× magnification (Bars in 20 μm scale). Non-significant *p*-value in the ANOVA test followed by Bonferroni.

first three criteria.

2.6. PCR Arrays

Total RNA from tumors induced by the 4 T1 cell line untreated (Control) and treated with nanoemulsion associated with visible light activation (NE-PcDoxo + PDT) were isolated using the RNeasy mini kit according to the manufacturer's instructions (Qiagen, Germany). Total RNA (2μg) from each group was reverse transcribed using the first-strand cDNA synthesis kit for RT-PCR (Qiagen, Germany), following the manufacturer's instructions. Nuclease-free water was used to dilute the amplified cDNA and was added to the RT^{2}qPCR SYBR Green Master Mix (Qiagen, Germany). After, 25μL of the experimental cocktail was added to each well to analyze the expression of 84 target genes for drug development and other 84 genes involved in apoptosis. For this, the Mouse Cancer Drug Targets RT^2 Profiler PCR Array (PAMM-507ZA) and Mouse Apoptosis RT^2 Profiler PCR Array (PAMM-012ZA) were used according to the manufacturer's instructions (Qiagen, Germany). Real-time PCR was performed on the Applied Biosystems 7300 Real-Time PCR System (Applied Biosystems, USA), and all experimental samples were in triplicate. Data from the PCR was collected, and differential expression of genes was analyzed by Qiagen Web Portal (https://www.qiagen.com/br/shop/genes-and-pathways/data-analysis-center-overview-page/).

2.7. Statistical Analysis

Data were previously subjected to descriptive analysis to determine normality. For samples with normal distribution, the different treatment groups were compared by Analysis of Variance (ANOVA) followed by the Bonferroni post-test. For those with non-normal distribution, the Kruskal-Wallis post-test was used for multiple comparisons. All values obtained were expressed as mean ± standard error using GraphPad Prism 7 (GraphPad Software Inc., San Diego, CA, USA). Any *p*-value of 0.05 was considered statistically significant.

3. Results

3.1. Efficiency of Nanoemulsions Combined with PDT

The analysis of the tumor growth curve showed that the treatment with NE-PcDoxo + PDT has a significant reduction of tumors in comparison to the other groups ($p < 0.01$) except for the NE-Pc + PDT + NE-Doxo group (Fig. 1). After euthanasia and tumor removal, a new *ex vivo* analysis was performed, in which a statistically significant difference was observed between tumor volume from mice treated with NE-PcDoxo + PDT ($p < 0.001$) (Fig. 2A, C). The same was observed for tumor weight ($p < 0.01$) (Fig. 2B) about the other groups (Fig. 2A, D). For this reason, only the combined treatment (NE-PcDoxo + PDT) was chosen for performing the PCR array experiments for differential gene expression evaluation.

3.2. Tumor Characterization

Tumor sections obtained were stained with HE (Fig. S1A). It was possible to identify three distinct cell patterns: (i) peripheral tumor regions with a predominance of proliferative cells (Fig. 3A; Fig. S1C), with a high supply of blood vessels (Fig. S1D); (ii) central regions of the tumor taken by initial necrosis, with evidence of pyknotic nuclei, chromatin condensation and cribriform patterns (Fig. 3B); and (iii) central regions

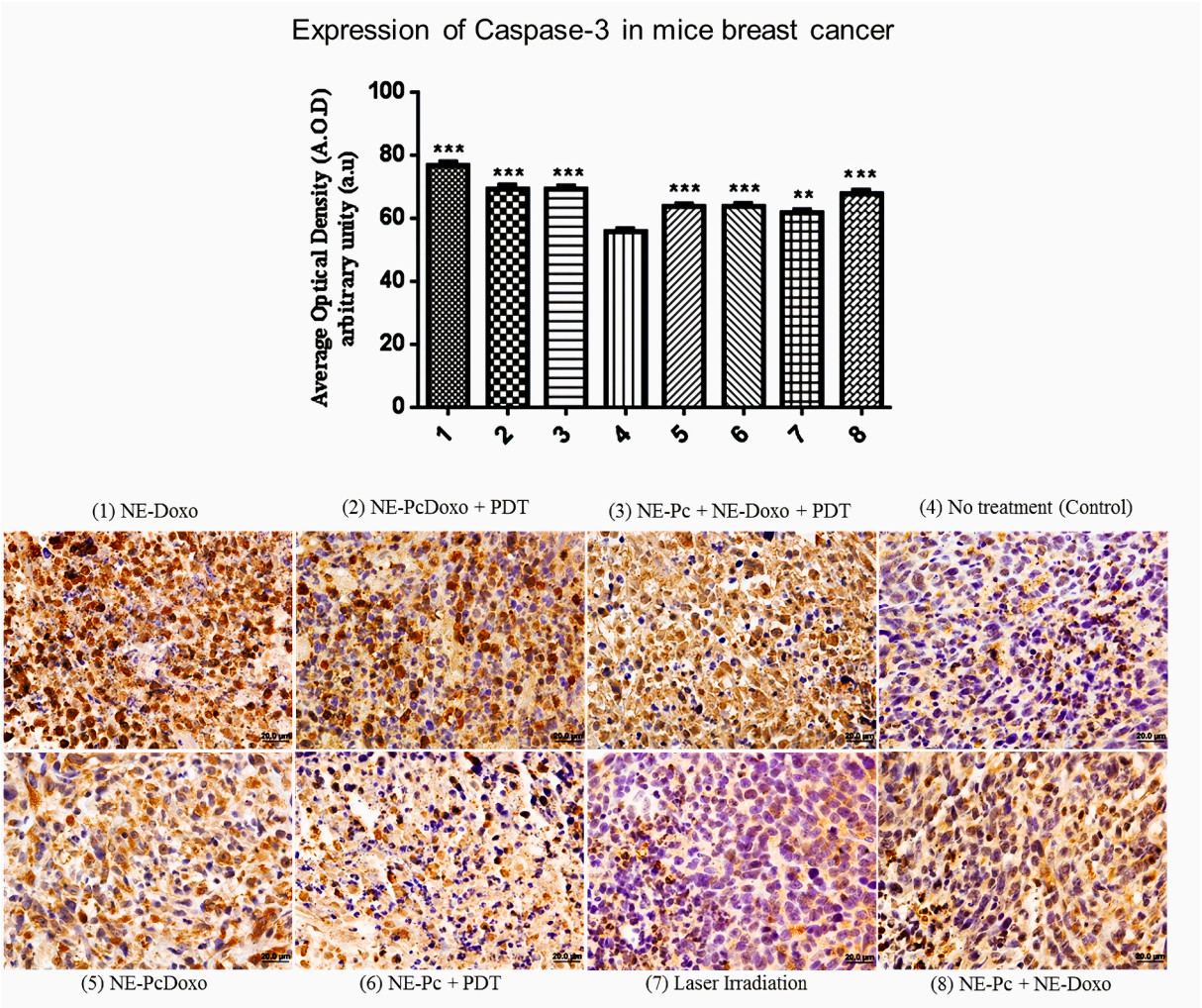

Fig. 7. Caspase-3 expression in tumor tissue from animals of the control group and subjected to different treatments. Micrographs in 40× magnification (Bars in 20 μm scale). Significant *p*-value in the ANOVA test followed by Bonferroni (± S.E.M. *** = $p < 0.0001$ compared to the control group; ** = $p < 0.001$).

with an advanced stage of massive tissue necrosis, showing karyolysis with swollen nuclei and a gradual or total loss of chromatin which may degenerate totally, also with hemosiderin deposits due to hemoglobin degradation caused by tissue hypoxia (Fig. 3C). These regions also showed extensive marking for caspase-3 (Fig. S1B).

Stereological analyses showed that the group NE-PcDoxo + PDT and the group NE-Pc + PDT + NE-Doxo showed a reduced proliferation area in comparison to the control group (40.8%), with an average proliferative area of 24.8% and 26.2%, respectively ($p < 0.0001$) (Fig. 4A). In contrast, these groups showed average rates of initial necrosis of 23.2% and 22.7% respectively ($p < 0.001$), similarly as the group that received laser irradiation (22.4%), showing an increase ($p < 0.01$) when compared to the control group (17.3%), as shown in Fig. 4B. Cellular regions showing complete karyolysis and, consequently, advanced necrosis stage were increased after NE-PcDoxo + PDT treatment (8.7%) when compared to control (5.3%) (p ⟨0,01). The opposite was observed for the group treated with NE-Pc + NE-Doxo, which had a decreased percentage area of advanced necrosis (1.2%) (p ⟨0,001) (Fig. 4C), confirming that in addition to chemical components, the laser was essential for an excellent anti-tumor effect. It is worth mentioning that treatments were only statistically different regarding the proportion of necrotic area since 4 T1 grown tumors are very aggressive and naturally present necrosis due to tissue hypoxia, which was also observed by Jurczyszyn et al. [16].

3.3. VEGF, CD31, Caspase-3 and Ki67 Protein Expression

VEGF expression decreased in NE-Doxo, NEPcDoxo + PDT, and NE-Pc + PDT + NE-Doxo treatments when compared to the control group (p < 0.0001) but showed a significant increase in NE-PcDoxo treatment (p ⟨0,0001) (Fig. 5). CD31 expression showed no statistical difference between treated and control groups neither by staining index and vascular micro density by the percentage of the marked area (Fig. 6). Although all groups had a significant increase of caspase-3 expression in comparison to control ($p < 0.0001$), the treatment with laser irradiation had less caspase-3 expression (p < 0.001) (Fig. 7). Expression of Ki67 showed a significant decrease in the groups NE-PcDoxo + PDT and NE-Pc + PDT + NE-Doxo when compared to control (p < 0.0001) (Fig. 8).

3.4. Differential Expression of Anticancer and Apoptosis Target Genes

The PCR array for drug targets evaluated 84 genes. From these, 6 genes showed decreased expression in the group that received intratumoral administration of conjugated nanoemulsion (NE-PcDoxo + PDT) compared to the control group (Table 1).

Four essential pro-apoptotic genes showed significant overexpression with a fold change ≥2: *ABL1*, *CD70*, *CRADD*, *FASL,* and *NME5*. In contrast, the anti-apoptotic genes *BCL2L10* and *NOL3* showed significantly decreased expression with fold change ≤2 (Table 2).

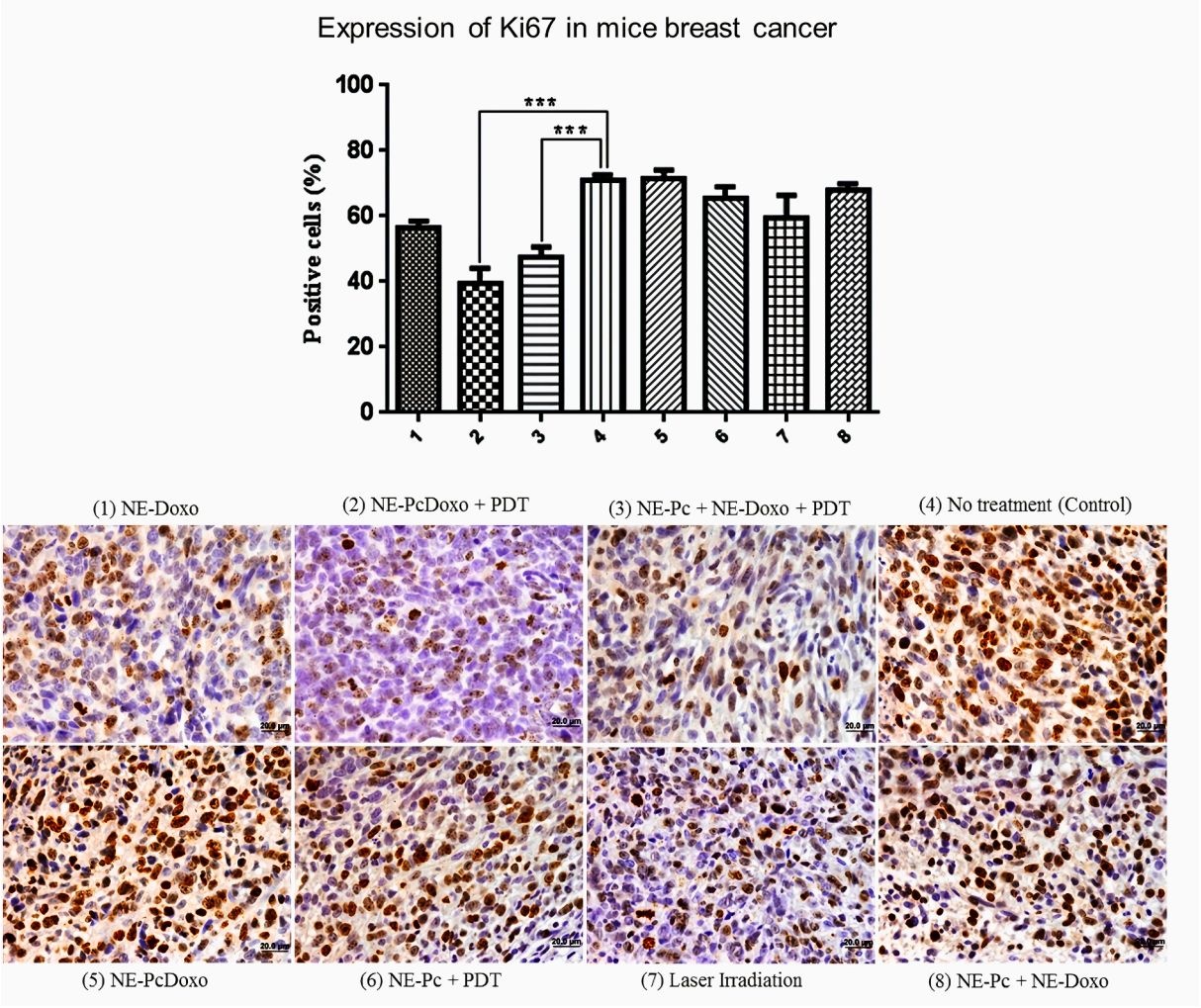

Fig. 8. Ki-67 expression in tumor tissue from animals of the control group and subjected to different treatments. Micrographs in 40× magnification (Bars in 20 μm scale). Significant p-value in the ANOVA test followed by Bonferroni (± S.E.M. *** = $p < 0.0001$ compared to the control group).

Table 1
Overview of the differentialy expressed genes related to the response to anti-tumor drugs in the tumors after the NE-PcDoxo+PDT treatment.

Gene symbol	Fold regulation	p-value
CDK2	**−2.33**	0.028511
ERBB2	**−2.07**	0.035297
FIGF	**−3.49**	0.038872
IGF2	**−3.50**	0.008166
PARP4	**−2.50**	0.041034
PGR	**−2.27**	0.019876

Table 2
Overview of the differentialy expressed apoptosis genes in the tumors after the NE-PcDoxo+PDT treatment.

Gene Symbol	Fold Regulation	p-value
ABL1	**6.13**	0.005706
BCL2L10	**−7.28**	0.000273
CD70	**2.90**	0.002337
CRADD	**2.19**	0.002036
FASL	**2.23**	0.011397
NME5	**2.44**	0.029019
NOL3	**−115,20**	0.001693

4. Discussion

PDT has shown significantly effective against several types of cancer [6]. ROS generated by PDT can react with biomolecules, and the damage to them can (i) irreversibly damage the tumor cells resulting in necrosis, apoptosis or autophagy, (ii) cause tumor ischemia (vascular injury), (iii) and activate the immune response against tumor antigens. Apoptosis and necrosis share common activation pathways and this implies that inhibition of apoptosis redirects cells to necrosis so that cells are destroyed regardless of the mechanism involved [6].

Our results demonstrated that there was a tumor regression after NE-PcDoxo + PDT treatment at the same time that extensive necrosis was observed. Jurczyszyn et al. [16] showed that a porphyrin derivative (DTDB-PDT) was able to reduce the size and cause 83.3% of necrosis in 4 T1 breast tumors. The tumor regression observed was more significant and may be explained by the long time from treatments until euthanasia and to the laser energy applied, which was higher. Photosensitizer porphyrin-derived + PDT led to histological changes correlated with acute necrosis with hyperchromic nuclei, karyolysis, pycnosis, and nuclear vacuoles in Walker tumors [17] and liposomal AlPc treatment for tongue tumors induced 90% of necrosis, characterized by an amorphous eosinophilic tissue without the integrity of the cytoplasmic membrane and absence of cell nucleus [18], both studies corroborating our findings.

The formation of blood vasculature is a mandatory step to sustain the

influx of essential nutrients to the tumor mass. Vascular endothelial growth factor (VEGF) is a potent angiogenic factor, which receptors are expressed in endothelial and tumor cells, where it can protect cells from apoptosis and increase their resistance to conventional chemotherapy and radiation therapy [19]. Our treatment with NE-PcDoxo + PDT decreased VEGF expression, providing a good prognostic than conventional therapies currently used. Similar results was described after PDT regimen which reduced size of tumors and the spread of metastases [20].

Apoptosis is a complex programmed cell death that includes several cell pathways and is initiated through the activation of death receptors or mitochondrial release of cytochrome *c* [21]. Xenotransplanted mice with colorectal cancer showed an increase in caspase-3 after treatment with PDT using Pc4 photosensitizer [22], corroborating our results. There are *in vitro* studies describing this pattern after PDT for different photosensitizers in BC [23,24]. Our study is unprecedented in the literature since it analyzes caspase-3 activity by immunohistochemistry *in vivo* using chemotherapeutic and photosensitizer association with PDT.

We found a significant decrease in Ki67 positive cells and these data corroborate previous *in vitro* results since it was observed that 4 T1 cells stopped in the subG1 phase after treatment, and this protein is not expressed in this stage of cell cycle [12]. A study observed a significant decrease of Ki67 expression in mice with BC treated with doxorubicin and chlorine e6 nanoparticles + PDT [25] corroborating our findings. Another regimen of ALA-PDT can inhibit the proliferation of A431 and COLO-16 cells and promote apoptosis. These factors correlate with tumor size [26], as observed in our study after NE-PcDoxo + PDT application.

Essential drug target genes were downregulated after NE-PcDoxo + PDT: *CDK2, ERBB2,* and *IGF2*. Cyclin-dependent kinase 2 (Cdk2) is a critical enzyme in the transition of cells from G1 to S phase, and evidence indicates that *CDK2* promotes hyperproliferation and is associated with poor prognosis in multiple cancer cells [27]. Patel et al. [28] demonstrated that inhibition of *CDK2* induces a potent and durable response against breast cancer cells. The *ERBB2* gene (also known as *HER2* or *NEU*) is overexpressed in about 30% of breast cancers and disrupts standard cellular control mechanisms, generating aggressive tumor cells. High expression of *ERBB2* is correlated with concomitant overexpression of *FIGF* in breast cancer [29] and our treatment proposed led to negative regulation of this gene concomitantly with *FIGF*.

The insulin-like growth factor II (*IGF2*) is the most intrinsically regulated of all characterized growth factors and it is well known for their mitogenic activities, so, IGFs can stimulate growth and differentiation in many tissues [30]. A study by Tominaga et al. [31] showed that *IGF2* overexpression increases the ability to initiate tumor in MCF7 cells. Therefore, a decrease in these genes expression after NE-PcDoxo + PDT confirm its efficiency.

Regarding the genes involved in the apoptosis pathway, *ABL1*, *CRADD*, *FASL, BCL2L10*, and *NOL3* are noteworthy in this study. The *ABL* oncogene encodes a tyrosine kinase distributed in the nucleus and cytoplasm of proliferating cells. In the nucleus, *c-ABL* activity is negatively regulated by the protein retinoblastoma and positively regulated by signs of DNA damage [32]. *CRADD* encodes an adapter protein containing a death domain (DD) motif similar to that of *FADD*. This protein recruits caspase 2 in cell death signal transduction complex, which includes tumor necrosis factor receptor 1 (TNFR1A) and RIPK1/RIP kinase; therefore, it acts by promoting apoptosis [33]. *FAS* (also known as Apo-1 or CD95), a potent member of the death receptor family, plays a crucial role in extrinsic apoptotic signaling in many cell types. Breast tumors exhibit negative *FAS* regulation or loss of function, conferring resistance to the death signals induced by the immune system [34]. The increased expression of these genes observed suggests cell death induction in breast tumors.

The B-cell lymphoma-2 protein family (BCL-2) is one of the primary regulators of apoptosis, and is located predominantly in mitochondria, the critical decision point of cytochrome *c* regulation and release [35]. *BCL2L10* is overexpressed in BC [36] and *NRH* homologous of *BCL2L10* was found to be overexpressed in >45% of a large cohort of invasive breast carcinomas, correlating with reduced metastasis-free survival and defined as a poor prognosis marker [37]. The *NOL3* gene encodes ARC protein (apoptosis repressor with CARD domain) and it has an anti-apoptotic function that regulates enzymatic activity of caspases −2,−8 and tumor suppressor protein p53, capable of specifically inhibiting both intrinsic and extrinsic cell death pathways [38]. Increased expression of *NOL3* was associated with glioblastoma progression due to decreased apoptosis [39] and the silencing of *NOL3* in BC mouse model led to a decrease in the primary tumor, limited the invasion and circulating cancer cells [40]. Therefore, NE-PcDoxo + PDT treatment was considerably able to decrease the expression of described genes, contributing to the activation of cell death pathways. These mechanisms are added to the promising results of the decrease in tumor volume and weight observed in the eligible treatment proposed.

5. Conclusion

Our results demonstrated tumor regression through apoptosis and extensive necrosis after NE-PcDoxo + PDT administration. Besides, we also observed a decrease in VEGF and Ki67 levels, decrease in some drug target genes expression, and an increase in the expression of genes involved in apoptosis pathway. Synergistic treatments involving photosensitizer and chemotherapy delivery plus PDT provided a good antitumor response. Thus, this combined therapy can considerably block tumor breast development, providing a better prognostic than conventional therapies currently used and is considered a promising solution among new targeted anti-tumor therapies.

Supplementary data to this article can be found online at https://doi.org/10.1016/j.jphotobiol.2021.112181.

Declaration of Competing Interest

The authors declare that they have no competing interests.

Acknowledgements

M.F.C thanks ……A.S.C thanks…..A.C.T. and H.L.P. thanks the State of São Paulo Research Foundation (FAPESP) Thematic project #2013/50181-1, and FAPESP 2020/04009-6. M.T.M thanks Brazilian Federal Agency for Support and Evaluation of Graduate Education (CAPES). We also thank Project PRONON-SIPAR #25000.077093/2015-86 for financial support.

References

[1] F. Bray, et al., Global cancer statistics 2018: GLOBOCAN estimates of incidence and mortality worldwide for 36 cancers in 185 countries, CA Cancer J. Clin. 68 (6) (2018) 394–424.
[2] E.S. McDonald, et al., Clinical diagnosis and management of breast cancer, J. Nucl. Med. 57 (Supplement 1) (2016) 9S–16S.
[3] S. Tran, et al., Cancer nanomedicine: a review of recent success in drug delivery, Clin. Trans. Med. 6 (1) (2017) 1–21.
[4] C. Lovelyn, A.A. Attama, Current state of nanoemulsions in drug delivery, J. Biomater. Nanobiotechnol. 2 (05) (2011) 626.
[5] A. Oniszczuk, et al., The potential of photodynamic therapy (PDT)—experimental investigations and clinical use, Biomed. Pharmacother. 83 (2016) 912–929.
[6] C.A. Robertson, D.H. Evans, H. Abrahamse, Photodynamic therapy (PDT): a short review on cellular mechanisms and cancer research applications for PDT, J. Photochem. Photobiol. B Biol. 96 (1) (2009) 1–8.
[7] L.A. Muehlmann, et al., Aluminum–phthalocyanine chloride associated to poly (methyl vinyl ether-co-maleic anhydride) nanoparticles as a new third-generation photosensitizer for anticancer photodynamic therapy, Int. J. Nanomedicine 9 (2014) 1199.
[8] C. Christowitz, et al., Mechanisms of doxorubicin-induced drug resistance and drug resistant tumour growth in a murine breast tumour model, BMC Cancer 19 (1) (2019) 1–10.
[9] Q. Hu, et al., Recent advances of cocktail chemotherapy by combination drug delivery systems, Adv. Drug Deliv. Rev. 98 (2016) 19–34.

[10] P. Parhi, C. Mohanty, S.K. Sahoo, Nanotechnology-based combinational drug delivery: an emerging approach for cancer therapy, Drug Discov. Today 17 (17–18) (2012) 1044–1052.
[11] E. Tabosa do Egito, et al., New techniques for preparing submicronic emulsions: application to amphotericin B, STP Pharma Sci. 4 (2) (1994) 155–162.
[12] N.M. Candido, et al., Combining photodynamic therapy and chemotherapy: improving breast cancer treatment with nanotechnology, J. Biomed. Nanotechnol. 14 (5) (2018) 994–1008.
[13] B.V. Jardim-Perassi, et al., Effect of melatonin on tumor growth and angiogenesis in xenograft model of breast cancer, PLoS One 9 (1) (2014), e85311.
[14] C. Bouzin, et al., Digital pathology: elementary, rapid and reliable automated image analysis, Histopathology 68 (6) (2016) 888–896.
[15] E. Weibel, Principles and methods for the morphometric study of the lung and other organs, Lab. Investig. 12 (1963) 131–155.
[16] K. Jurczyszyn, et al., Assessment of in vivo experiments: the newly synthesized porphyrin with proper light source enhanced effectiveness of PDT comparing to 5-ALA-mediated PDT, Photodiagn. Photodyn. Ther. 18 (2017) 179–184.
[17] I.-P. Laszlo, et al., The in vivo modulatory effects of Cornus mas extract on photodynamic therapy in experimental tumors, Photodiagn. Photodyn. Ther. 30 (2020) 101656.
[18] J.P.F. Longo, et al., Photodynamic therapy with aluminum-chloro-phtalocyanine induces necrosis and vascular damage in mice tongue tumors, J. Photochem. Photobiol. B Biol. 94 (2) (2009) 143–146.
[19] H.L. Goel, A.M. Mercurio, VEGF targets the tumour cell, Nat. Rev. Cancer 13 (12) (2013) 871–882.
[20] I. Lisnjak, et al., Effect of photodynamic therapy on tumor angiogenesis and metastasis in mice bearing Lewis lung carcinoma, Exp. Oncol. 27 (4) (2005) 333–335.
[21] C.A. Pettigrew, T.G. Cotter, Deregulation of cell death (apoptosis): implications for tumor development, Discov. Med. 8 (41) (2009) 61–63.
[22] C.M. Whitacre, et al., Photodynamic therapy with the phthalocyanine photosensitizer pc 4 of SW480 human colon cancer xenografts in athymic mice, Clin. Cancer Res. 6 (5) (2000) 2021–2027.
[23] B.P. George, H. Abrahamse, N.M. Hemmaragala, Anticancer effects elicited by combination of Rubus extract with phthalocyanine photosensitiser on MCF-7 human breast cancer cells, Photodiagn. Photodyn. Ther. 19 (2017) 266–273.
[24] F.C. Machado, et al., Effect of curcumin-nanoemulsion associated with photodynamic therapy in breast adenocarcinoma cell line, Bioorg. Med. Chem. 27 (9) (2019) 1882–1890.
[25] D. Hu, et al., Oxygen-generating hybrid polymeric nanoparticles with encapsulated doxorubicin and chlorin e6 for trimodal imaging-guided combined chemo-photodynamic therapy, Theranostics 8 (6) (2018) 1558.
[26] L. Qiao, et al., ALA-PDT inhibits proliferation and promotes apoptosis of SCC cells through STAT3 signal pathway, Photodiagn. Photodyn. Ther. 14 (2016) 66–73.
[27] S. Akli, et al., Cdk2 is required for breast cancer mediated by the low-molecular-weight isoform of cyclin E, Cancer Res. 71 (9) (2011) 3377–3386.
[28] P. Patel, et al., Dual inhibition of CDK4 and CDK2 via targeting p27 tyrosine phosphorylation induces a potent and durable response in breast cancer cells, Mol. Cancer Res. 16 (3) (2018) 361–377.
[29] W. Yang, et al., ErbB2 overexpression correlates with increased expression of vascular endothelial growth factors A, C, and D in human breast carcinoma, Cancer: Interdiscip. Int. J. Am. Cancer Soc. 94 (11) (2002) 2855–2861.
[30] W. Chao, P.A. D'Amore, IGF2: epigenetic regulation and role in development and disease, Cytokine Growth Factor Rev. 19 (2) (2008) 111–120.
[31] K. Tominaga, et al., Addiction to the IGF2-ID1-IGF2 circuit for maintenance of the breast cancer stem-like cells, Oncogene 36 (9) (2017) 1276–1286.
[32] J.Y. Wang, Regulation of cell death by the Abl tyrosine kinase, Oncogene 19 (49) (2000) 5643–5650.
[33] L. Lo Muzio, et al., Expression and prognostic significance of apoptotic genes in oral squamous cell carcinoma, Mol. Carcinog. 53 (4) (2014) 264–271.
[34] W. Wang, et al., Polymorphisms of the FAS and FASL genes and risk of breast cancer, Oncol. Lett. 3 (3) (2012) 625–628.
[35] J.T. Opferman, A. Kothari, Anti-apoptotic BCL-2 family members in development, Cell Death Differ. 25 (1) (2018) 37–45.
[36] M. Krajewska, et al., Bcl-B expression in human epithelial and nonepithelial malignancies, Clin. Cancer Res. 14 (10) (2008) 3011–3021.
[37] A. Nougarede, et al., Breast Cancer targeting through inhibition of the endoplasmic reticulum-based apoptosis regulator Nrh/BCL2L10, Cancer Res. 78 (6) (2018) 1404–1417.
[38] G. Kung, et al., A novel role for the apoptosis inhibitor ARC in suppressing TNF α-induced regulated necrosis, Cell Death Differ. 21 (4) (2014) 634–644.
[39] D.S. Ziegler, et al., Resistance of human glioblastoma multiforme cells to growth factor inhibitors is overcome by blockade of inhibitor of apoptosis proteins, J. Clin. Invest. 118 (9) (2008) 3109–3122.
[40] C.M. Medina-Ramirez, et al., Apoptosis inhibitor ARC promotes breast tumorigenesis, metastasis, and chemoresistance, Cancer Res. 71 (24) (2011) 7705–7715.